Douglas–Gunn Method Applied to Dosimetric Assessment in Magnetic Resonance Imaging

Douglas–Gunn method applied to dosimetric assessment in magnetic resonance imaging

Authors

Alessandro Arduino[a,b], Oriano Bottauscio[b]*, Mario Chiampi[a], Luca Zilberti[b]

Author affiliation

[a] Dipartimento Energia – Politecnico di Torino – Corso Duca degli Abruzzi, 24 – 10129 Torino, Italia

[b] Istituto Nazionale di Ricerca Metrologica (INRIM) – Strada delle Cacce, 91 – 10135 Torino, Italia

* Correspondence should be addressed to: o.bottauscio@inrim.it

Published journal article available at DOI: https://doi.org/10.1109/TMAG.2017.2658021

Douglas–Gunn Method Applied to Dosimetric Assessment in Magnetic Resonance Imaging

Alessandro Arduino[1,2], Oriano Bottauscio[2], *IEEE Senior Member*, Mario Chiampi[1] and Luca Zilberti[2]

[1]Dipartimento Energia – Politecnico di Torino – Corso Duca degli Abruzzi, 24 – 10129 Torino, Italia
[2]Istituto Nazionale di Ricerca Metrologica (INRIM) – Strada delle Cacce, 91 – 10135 Torino, Italia

The Douglas–Gunn method has been applied to the solution of Pennes' bioheat equation to estimate the heating of bulk metallic prostheses caused by the energy deposition due to the gradient magnetic field of a magnetic resonance imaging (MRI) scanner. The proposed method has been implemented to work on a graphic processing unit (GPU) and the accuracy and numerical efficiency has been compared with the explicit Euler scheme. As an example of application, the heating of a realistic hip prosthesis during the execution of a 3D true fast imaging with steady precession (True-FISP) MRI sequence has been finally evaluated.

***Index Terms*—Biomedical computing, Numerical analysis, Magnetic resonance imaging, Douglas–Gunn method.**

I. Introduction

THE THERMAL effects induced in patients' body by the exposure to the electromagnetic fields (EMFs) generated during magnetic resonance imaging (MRI) sessions are an element of concern. The radiofrequency (RF) EMF, used to trigger the Larmor precession phenomenon, can cause thermal issues associated to localized hotspots of dissipated power density in case of ultra-high field MRI [1], or in presence of metallic medical devices (*e.g.*, implanted wires [2-5]). Moreover, the EMFs generated by the gradient coils (GCs) may produce a significant thermal effect in presence of bulky metallic prostheses, because of Joule losses [6-9].

For both the RF and the GCs EMFs, the time scale of the induced thermal effect is much larger than the electromagnetic one. In addition, due to the limited temperature increase (few degrees), the coefficients of both the electromagnetic and thermal models can be assumed independent on temperature.

These considerations allow decoupling the two problems, solving them sequentially. The power densities developed by the EMFs are estimated by a hybrid finite element–boundary element (FE-BE) method [7, 10], and then used for driving the transient thermal problem. The latter solution is here approximated by an original finite difference method (FDM) using Douglas–Gunn (DG) time split [11], implemented to work on a Graphic Processing Unit (GPU). The DG time split has been chosen in virtue of its stability condition, less restrictive than an explicit method, and its memory consumption, smaller with respect to a classical implicit technique. The proposed method is applied to the estimate of the thermal effects induced by the GCs EMFs in the tissues surrounding a metallic hip prosthesis. The results are compared, in terms of accuracy and numerical efficiency, to those given by a homemade explicit Euler scheme and the commercial software Semcad X [12]. Finally, the method is applied to a realistic case, namely the evaluation of temperature increase in a patient with unilateral hip prosthesis when subjected to a realistic GC sequence adopted during an MRI session.

Manuscript received November 20, 2016.First Revision January 4, 2017.
Corresponding author: Oriano Bottauscio (e-mail: o.bottauscio@inrim.it).
All authors contributed equally to this work.
Digital Object Identifier (inserted by IEEE).

II. Problem formulation

The predicted temperature increase is usually small enough to assume that the parameters of both the electromagnetic and thermal problems do not vary with temperature. Thus, also by virtue of the different time scales of the two phenomena (from milliseconds to minutes), the electromagnetic and the thermal problems can be decoupled and solved sequentially.

A. Electromagnetic problem

The electromagnetic problem is driven by the magnetic field $\boldsymbol{H}_s$ produced by the sources and develops within a magnetically homogeneous domain with vacuum magnetic permeability. The problem is studied in frequency domain, through a $\boldsymbol{T}$-Ω formulation ($\boldsymbol{T}$: electric vector potential, Ω: magnetic scalar potential) handled by a homemade FE-BE code [6,10]. In the subdomain where electromagnetic induction takes place (*i.e.*, the internal FE region), the induced current density is $\boldsymbol{J} = \nabla\times\boldsymbol{T}$ and the total magnetic field is $\boldsymbol{H} = \boldsymbol{H}_s + \boldsymbol{T} + \nabla\Omega$. In this specific implementation, unlike [6,10], the projections of $\boldsymbol{T}$ on the mesh edges are adopted as FE unknowns, together with the nodal values of Ω. In the external BE region, $\boldsymbol{J}$ is assumed to be null, $\boldsymbol{T}$ is not defined and the magnetic field is simply given by $\boldsymbol{H} = \boldsymbol{H}_s + \nabla\Omega$. Here, Ω satisfies the Laplace equation and goes to zero at infinity; its normal derivative, considered uniform over each BE, is used as unknown. At the FE-BE interface, the continuity of the normal component of the magnetic field is enforced and the tangential components of $\boldsymbol{T}$ (*i.e.*, the contributions of the edges along the boundary) are set to zero to bound $\boldsymbol{J}$ within the FE region. Since no additional constraint is applied to $\boldsymbol{T}$, the formulation is ungauged but can be solved through a GMRES algorithm. The code is implemented to run on GPUs, similar to the scheme described in [13].

B. *Thermal problem*

The thermal problem is modelled by Pennes' equation [14] written in terms of temperature elevation ϑ with respect to the temperature of the body before the exposure [15,16]:

$$\rho c_p \, \partial\vartheta/\partial t = \nabla\cdot(\lambda\nabla\vartheta) - h_b\vartheta + P_{em}, \quad (1)$$

Here P_{em} is the volume power density produced by the EMF, ρc_p is the volumetric heat capacity, λ is the thermal conductivity and h_b is the blood perfusion coefficient. This equation works also in implanted prostheses, where h_b is null. Robin boundary conditions are enforced to model the heat transfer toward the external environment,

$$\lambda\,\partial\vartheta/\partial n\big|_{\partial V} = -h_{amb}\vartheta, \quad (2)$$

where h_{amb} is the heat exchange coefficient and n indicates the direction normal to the boundary (outward-directed).

In order to introduce the DG time split, the problem has to be semi-discretized in space on a structured Cartesian mesh, using a FDM with a second order centered scheme. The resulting ordinary differential equation is approximated by the Crank–Nicolson (CN) method, with error $O(\Delta t^2)$, to obtain

$$\left(I - \frac{\Delta t}{2}A_x - \frac{\Delta t}{2}A_y - \frac{\Delta t}{2}A_z\right)\boldsymbol{\vartheta}^{n+1} - \frac{\Delta t}{2}R\boldsymbol{\vartheta}^{n+1} = \\ = \left(I + \frac{\Delta t}{2}A_x + \frac{\Delta t}{2}A_y + \frac{\Delta t}{2}A_z\right)\boldsymbol{\vartheta}^{n} + \frac{\Delta t}{2}R\boldsymbol{\vartheta}^{n} + \boldsymbol{f}^{n}, \quad (3)$$

where Δt is the time step, $\boldsymbol{\vartheta}^n$ is the column vector collecting the approximate solution in the mesh nodes at the instant $t^n = n\Delta t$, I is the identity matrix, the matrices A_x, A_y and A_z discretize the diffusion term in the x-, y- and z-direction respectively, matrix R discretizes the perfusion, and $\boldsymbol{f}^n = \Delta t P_{em}{}^{n+1/2}/\rho c_p$. The matrices that discretize the diffusion in each direction can be introduced thanks to the regularity of the mesh. By exploiting the polynomial relation

$$(1+x+y+z) = (1+x)(1+y)(1+z) - (xy + xz + yz + xyz) \quad (4)$$

equation (3) can be approximated with an error $O(\Delta t^2)$, having the same magnitude of the error introduced by CN, as

$$\left(I - \frac{\Delta t}{2}A_x\right)\left(I - \frac{\Delta t}{2}A_y\right)\left(I - \frac{\Delta t}{2}A_z\right)\boldsymbol{\vartheta}^{n+1} - \frac{\Delta t}{2}R\left(\boldsymbol{\vartheta}^{n+1} + \boldsymbol{\vartheta}^{n}\right) = \\ = \left(\left(I + \frac{\Delta t}{2}A_x\right)\left(I + \frac{\Delta t}{2}A_y\right)\left(I + \frac{\Delta t}{2}A_z\right) - \frac{\Delta t^3}{4}A_xA_yA_z\right)\boldsymbol{\vartheta}^{n} + \\ - \frac{\Delta t^2}{4}\left(A_x + A_y - \frac{\Delta t}{2}A_xA_y\right)R\left(\boldsymbol{\vartheta}^{n+1} + \boldsymbol{\vartheta}^{n}\right) + \boldsymbol{f}^{n},$$

which can be finally split in the system of vectorial equations

$$\begin{cases} \left(I - \frac{\Delta t}{2}A_x\right)\boldsymbol{\vartheta}^{*} = \left(I + \frac{\Delta t}{2}A_x + \Delta t A_y + \Delta t A_z\right)\boldsymbol{\vartheta}^{n} + \Delta t R\boldsymbol{\vartheta}^{n} + \boldsymbol{f}^{n} \\ \left(I - \frac{\Delta t}{2}A_y\right)\boldsymbol{\vartheta}^{**} = \boldsymbol{\vartheta}^{*} - \frac{\Delta t}{2}A_y\boldsymbol{\vartheta}^{n} \\ \left(I - \frac{\Delta t}{2}A_z\right)\boldsymbol{\vartheta}^{n+1} = \boldsymbol{\vartheta}^{**} - \frac{\Delta t}{2}A_z\boldsymbol{\vartheta}^{n} + \frac{\Delta t}{2}R\left(\boldsymbol{\vartheta}^{n+1} - \boldsymbol{\vartheta}^{n}\right) \end{cases} \quad (5)$$

where $\boldsymbol{\vartheta}^*$ and $\boldsymbol{\vartheta}^{**}$ are two fictitious intermediate solutions [11].

Unlike the starting CN method, the DG time split is stable when condition $\Delta t/\Delta s^2 \le k$ is verified for some constant k, and the spatial step Δs [17]. This condition is analogous to the one of the explicit Euler (EE) scheme, but usually k is higher for the DG time split.

- *Transfer fixed data from CPU to GPU memory*
- *For each time instant, do*
  - *Transfer to GPU the power density*
  - *Launch the GPU kernel where each thread*
    - *Compute the rhs and apply the Thomas algorithm to a subsystem of the first vectorial equation in Eqn. (5)*
    - *Compute the rhs and apply the Thomas algorithm to a subsystem of the second vectorial equation in Eqn. (5)*
    - *Compute the rhs and apply the Thomas algorithm to a subsystem of the third vectorial equation in Eqn. (5)*
  - *Transfer to CPU the updated solution*

Fig. 1. Pseudocode of CPU-GPU implementation.

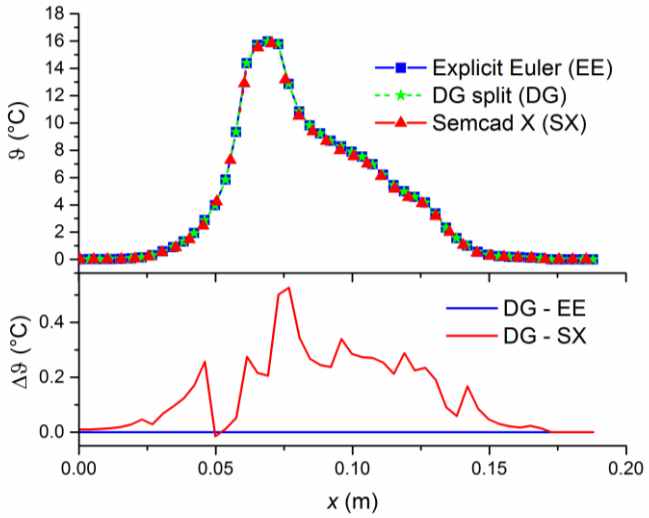

Fig. 2. Temperature elevation (upper plot) along a line passing through the maximum, computed by the three numerical methods on a cubic mesh of 1 mm side. In the lower plot the differences between results.

In each row, the only non-null elements of matrices A_x, A_y and A_z refer to nodes belonging to the same line directed respectively as x, y and z. Consequently, each system of (5) consists in as many independent tridiagonal subsystems as the number of lines along the considered direction presented in the mesh. This fact enables a parallel implementation of the method: each vectorial equation of (5) is split among the computational units that simultaneously apply the Thomas algorithm to solve the tridiagonal subsystems [18]; then, the solutions are rearranged for the next equation. Because of the absence of conditional statements in Thomas algorithm, the proposed strategy has been efficiently implemented to work on a GPU within the PGI CUDA Fortran environment [19], as described in the pseudocode of Fig. 1.

III. VALIDATION AND COMPARISONS

To test the proposed method, the temperature increase of a metallic hip prosthesis and surrounding biological tissues produced by the exposure to the GCs EMFs has been studied. To this purpose, the anatomical human model Duke [20], with biological tissue properties given by the IT'IS database [21], has been modified to include a hip prosthesis. The implant is composed of acetabular shell, femoral head and stem, made of a non-magnetic metallic CoCrMo alloy (electrical

TABLE I
EXECUTION TIME OF THE PROPOSED METHOD COMPARED TO EXPLICIT EULER AND A COMMERCIAL SOFTWARE

Mesh size	Explicit (CPU)	Explicit (GPU)	DG-split (CPU)	DG-split (GPU)	Semcad X (GPU)
2 mm	5219 s	4052 s	149 s	67 s	156 s
1 mm	-	111963 s	5070 s	2151 s	5499 s

conductivity σ = 1.16 MS/m, λ = 14 W/m/°C, ρc_p = 3.8 MJ/m^3/°C), and a liner of polyethylene located between the acetabular shell and the femoral head (σ = 0, λ = 0.47 W/m/°C, ρc_p = 1.8 MJ/m^3/°C). The top of the femoral head is placed at 300 mm from the isocentre (*i.e.*, the MRI exam involves the abdomen) to simulate relatively worst conditions [22].

A conventional system of three GCs, typical ofa tubular MRI scanner has been considered. Each coil can produce a linear variation of the longitudinal field equal to 30 mT/m in a diameter spherical volume (DSV) of 500 mm. The power density dissipated inside the implant when all GCs are fed in phase with a sinusoidal current at 1 kHz has been computed applying the FE-BE method to a mesh made of 0.5 mm cubic voxels. The thermal problem has been then solved on the whole domain, including prosthesis and surrounding tissues, discretized with 1 mm voxels, computing the temperature elevation after a continuous exposure of 90 minutes. It has been empirically observed that k = 1.5 s/mm^2 is sufficient to guarantee the stability of the proposed DG time split, against k = 0.045 s/mm^2 for the EE scheme. The solutions obtained applying the EE scheme, the DG time split and the Semcad X proprietary code are presented in Fig. 2, along a line passing through the maximum temperature elevation. The maximum difference between DG and Semcad X results is lower than 3% (bottom diagram in Fig. 2), while DG and EE results are almost coincident. The adopted time steps are 0.025 s for the EE scheme, 1.5 s for the DG time split and 0.045 s for Semcad X. The three solvers run on the same workstation, equipped with an Intel Xeon CPU E5-2650 v3 and the GPU NVIDIA Quadro K6000. The homemade EE scheme operating in CPU has not been run due to the excessive processing time. Thus, for a complete comparison, the computations are repeated with a 2 mm cubic mesh (with time steps increased by a factor 4). Table 1 summarizes the execution times of each method run on both CPU and GPU. It is worth noting that, despite it is implicit, the computational cost of the proposed method increases linearly with the number of time steps and voxels, because Thomas algorithm is linear with the dimension of the system. This fact is evidenced in Table 1, where, passing from 2 mm to 1 mm, the execution times are multiplied by 32 (the number of voxels and time steps increase by a factor 8 and 4, respectively).

IV. Application to a Case Study

The DG time split has been applied to the study of the heating of the hip prosthesis during the execution of the 3D true fast imaging with steady precession (True-FISP) sequence, described in [8] and shown in Fig. 3. The repetition time (TR) is 6.4 ms, leading to a fundamental frequency of about 156 Hz. The Fourier series of the waveforms of each

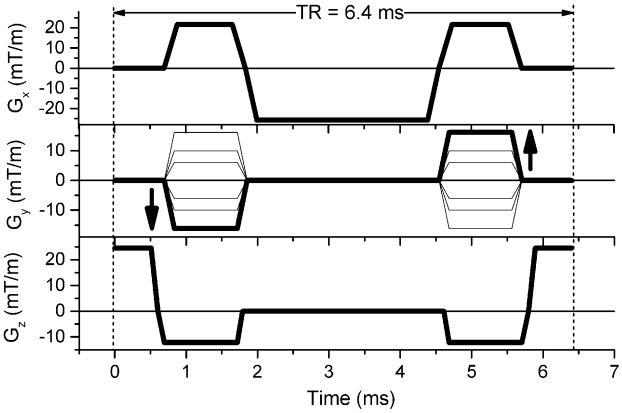

Fig. 3. Gradient switching in the 3D-True-FISP sequence (see Ref. [8]). The repetition time (TR) is 6.4 ms.

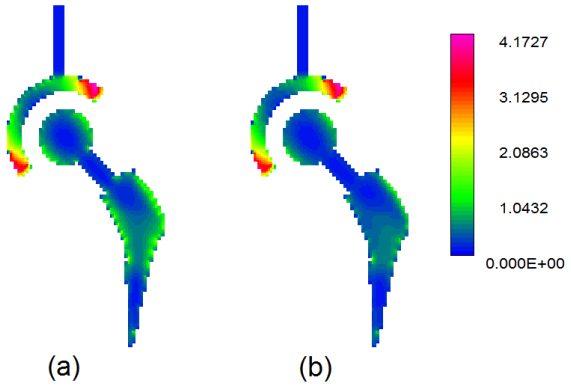

Fig. 4. Spatial distribution of power density (W/kg) in the central section of the implant for the two extreme supply conditions: a) y-coil producing the maximum gradient (16 mT/m), b) y-coil switched-off.

coil has been truncated at the 31st harmonic.

A set of electromagnetic simulations have been performed supplying each GC with an electric current producing the corresponding harmonic content of the gradient waveform and the results have been superposed considering two extreme conditions: the one (#1) with the amplitude of the G_y gradient at the maximum level (16 mT/m) and the one (#2) with the y-coil switched-off. The spatial distributions of the power density (per mass unit) within a central section of the implant are shown in Fig. 4 for the two cases mentioned above.

Thermal simulations have been run for both the extreme supply conditions of G_y gradient, considering and exposure time of 400 s. Simulations have been performed on the considered domain discretized with 2 mm cubic voxels, assuming a time step of 2 s with the DG time split and a time step of 0.03 s with the EE scheme. The computational times are 5 minutes for the DG scheme and 87 minutes for the EE scheme, adopting the GPU implementation on a Kepler K40 NVIDIA card.

The solutions obtained by the two schemes are completely superposed. The time evolutions of the temperature increase in the hottest point, obtained with y-coil supplies #1 and #2 are shown in Fig. 5. The limited discrepancies between the two cases prove the reduced role of the *y*-coil in the implant

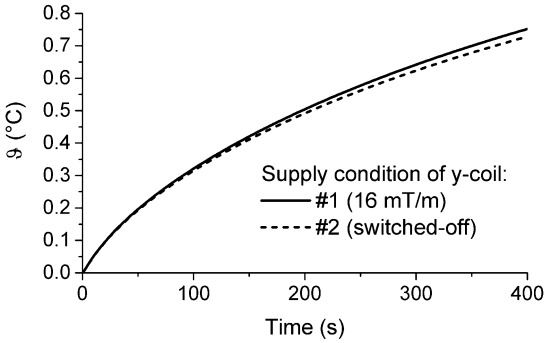

Fig. 5. Time evolution of ϑ in the point of maximum temperature elevation for the two extreme supply conditions: a) y-coil producing the maximum gradient (16 mT/m), b) y-coil switched-off.

heating for this type of sequence. Finally, the maps in Fig. 6 present the time evolution of the spatial distribution of ϑ in the central section of the implant. Such pictures clearly indicate that the implant starts to heat from the extreme parts of the acetabular cup. At the end of the entire sequence (t = 400 s), the whole cup reaches a temperature increase of about 0.7 °C and the heating starts to diffuse in the surrounding tissues. If the exposure time is increased up to the thermal steady state (which occurs after about 25 minutes), the heat diffuses within the implant and in the surrounding tissues, leading to the spatial distribution reported in the last image, with a maximum ϑ of about 1.4 °C.

V. CONCLUSIONS

In this work, the accuracy and numerical efficiency of the Douglas–Gunn method has been tested for the solution of Pennes' bioheat equation applied to dosimetric analysis of human exposure during MRI sessions. The analysis has evidenced the high efficiency of the DG time split and its linear scalability with the number of time steps and the number of voxels, thanks to the adoption of the Thomas algorithm for the system solution.

The proposed approach is proved to be conveniently implemented for running on GPU, allowing its applicability to the study of realistic dosimetric problems with high-resolution human body models, similar the one proposed in Section IV.

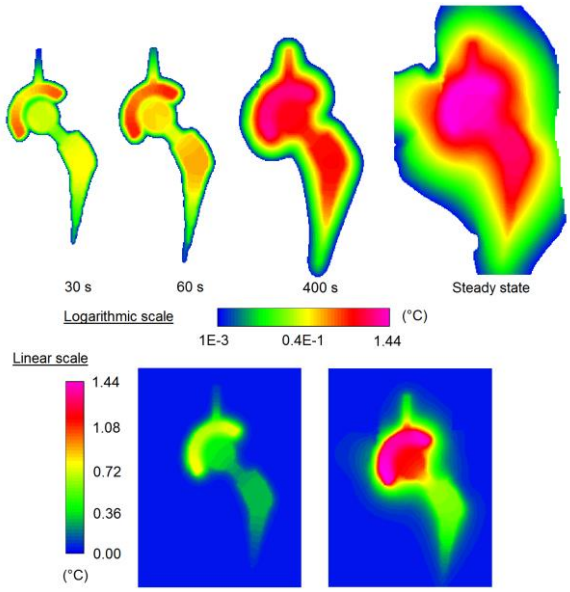

Fig. 6. Spatial distribution of ϑ (°C) in the central section of the implant and in the surrounding tissues for the supply condition of y-coil #1. In the figures above, the time evolution in logarithmic scale cut below 10^{-3} °C. In the figures below, the distribution at 400 s and at steady state in linear scale.

REFERENCES

[1] R. Lattanzi, D. K. Sodickson, A. K. Grant, and Y. Zhu, "Electrodynamic constraints on homogeneity and radiofrequency power deposition in multiple coil excitations," *Magn. Reson. Med.*, vol. 61, pp. 315–334, 2009.

[2] S. M. Park, R. Kamondetdacha, and J. A. Nyenhuis, "Calculation of MRI-induced heating of an implanted medical lead wire with an electric field transfer function," *J. Magn. Reson. Imag.*, vol. 26, pp. 1278–1285, 2007.

[3] A. R. Rezai *et al.*, "Neurostimulation systems for deep brain stimulation: in vitro evaluation of magnetic resonance imaging-related heating at 1.5 tesla," *J. Magn. Reson. Imag.*, vol. 15, pp. 241–250, 2002.

[4] E Neufeld, S Kuhn, G Szekely and N Kuster, "Measurement, simulation and uncertainty assessment of implant heating during MRI," *Phys. Med. Biol.*, vol. 54, pp. 4151–4169, 2009.

[5] S. M. Park, *et al.*, "MRI safety: RF-induced heating near straight wires," *IEEE Trans. Magn.*, vol. 41, no. 10, pp. 4197-4199, Oct. 2005.

[6] L. Zilberti *et al.*, "Collateral thermal effect of MRI-LINAC gradient coils on metallic hip prostheses," *IEEE Trans. Magn.*, vol. 50, no. 11, art. 5101704, Nov. 2014.

[7] L Zilberti *et al.*, "Numerical prediction of temperature elevation induced around metallic hip prostheses by traditional, split, and uniplanar gradient coils," *Magn. Reson. Med.*, vol. 74, pp. 272–279, Jul. 2015.

[8] H. Graf, G. Steidle, and F. Schick, "Heating of Metallic Implants and Instruments Induced by Gradient Switching in a 1.5-Tesla Whole-Body Unit," *J. Magn. Reson. Imag.*, vol. 26, pp. 1328–1333, 2007.

[9] L. Zilberti, A. Arduino, O. Bottauscio, and M. Chiampi, "The Underestimated Role of Gradient Coils in MRI Safety," *Magn. Reson. Med.*, in press. DOI 10.1002/mrm.26544.

[10] O. Bottauscio, M. Chiampi, J. Hand, and L. Zilberti, "A GPU Computational Code for Eddy-Current Problems in Voxel-Based Anatomy," *IEEE Trans. Magn.*, vol. 51, no. 3, art. 5100904, Mar. 2015.

[11] J. Douglas, and J. E. Gunn, "A general formulation of alternating direction methods. Part I. Parabolic and Hyperbolic Problems," *Numerische Mathematik*, vol. 6, pp. 428–453, 1964.

[12] SEMCAD, SPEAG – Schmid & Partner Engineering AG (see http://www.semcad.com).

[13] O. Bottauscio, M. Chiampi, and L. Zilberti, "Massively Parallelized Boundary Element Simulation of Voxel-Based Human Models Exposed to MRI Fields," *IEEE Trans. Magn.*, vol. 50, no. 2, art. 7025504, Feb. 2014.

[14] H. H. Pennes, "Analysis of tissue and arterial blood temperatures in the resting human forearm," *J. Appl. Physiol.*, vol. 1, no. 2, pp. 93–122, Aug. 1948.

[15] L. Zilberti, A. Arduino, O. Bottauscio, and M. Chiampi, "Parametric analysis of transient skin heating induced by terahertz radiation," *Bioelectromagn.*, vol. 35, pp. 314–323, 2014.

[16] O. Bottauscio, M. Chiampi, L. Zilberti, "Thermal analysis of Human Tissues Exposed to Focused Beam THz Radiations," *IEEE Trans. Magn.*, vol. 51, art. 7400504, March 2015.

[17] K. V. Voronin, and Y. M. Laevsky, "On the stability of some flux splitting schemes," *Num. Anal. Appl.*, vol. 8, no. 2, pp. 113–121, 2015.

[18] A. Quarteroni, R. Sacco, and F. Saleri, *Numerical mathematics*. New York, NY: Springer-Verlang, 2000.

[19] (2016) [Online]. Available: http://www.pgroup.com/resources/cudafortran.htm

[20] A. Christ, *et al.*, "The Virtual Family—development of surface-based anatomical models of two adults and two children for dosimetric simulations," *Phys. Med. Biol.*, vol. 55, pp. N23–N38, 2010.

[21] (2016) IT'IS Database for thermal and electromagnetic parameters of biological tissues. [Online]. Available: http://www.itis.ethz.ch/database

[22] L. Zilberti, *et al.*, "Power deposition into a metallic hip prosthesis exposed to switched gradient fields," Proc Int. Soc. Magn. Reson. Med. Sci. Meet Exhib. Int. Soc., Singapore, May 2016, ID 2225.